nature neuroscience

State and location dependence of action potential metabolic cost in cortical pyramidal neurons

Stefan Hallermann[1,2], Christiaan P J de Kock[3], Greg J Stuart[4] & Maarten H P Kole[4,5]

Action potential generation and conduction requires large quantities of energy to restore Na^+ and K^+ ion gradients. We investigated the subcellular location and voltage dependence of this metabolic cost in rat neocortical pyramidal neurons. Using Na^+/K^+ charge overlap as a measure of action potential energy efficiency, we found that action potential initiation in the axon initial segment (AIS) and forward propagation into the axon were energetically inefficient, depending on the resting membrane potential. In contrast, action potential backpropagation into dendrites was efficient. Computer simulations predicted that, although the AIS and nodes of Ranvier had the highest metabolic cost per membrane area, action potential backpropagation into the dendrites and forward propagation into axon collaterals dominated energy consumption in cortical pyramidal neurons. Finally, we found that the high metabolic cost of action potential initiation and propagation down the axon is a trade-off between energy minimization and maximization of the conduction reliability of high-frequency action potentials.

Fast electrical signaling in the brain uses action potentials and is associated with a substantial metabolic cost[1]. Given that resources are limited, the metabolic cost associated with action potential signaling is thought to have been important in the evolution of the biophysical properties of ion channels, of neural coding schemes and, ultimately, of neuronal number and/or brain size[2–7]. It has been estimated that, for each action potential in a rodent cortical pyramidal neuron, on the order of ~400×10^6 ATP molecules are required to restore the Na^+ and K^+ gradient via the Na^+/K^+ ATPase, making action potential signaling the second largest metabolic cost associated with mammalian brain function after synaptic transmission[1,6]. These estimates are based on studies of action potential signaling in the squid giant axon and frog node of Ranvier (NoR), which show that there is substantial overlap between Na^+ influx and K^+ efflux during an action potential, cancelling out the effect of Na^+ flux on membrane polarization. As a result, the Na^+ influx during action potential generation in these axons is about fourfold larger than the theoretical minimum needed to produce the action potential voltage waveform, potentially wasting energy resources[8,9].

Recently, the extent of excess Na^+ influx compared with K^+ efflux was experimentally determined in presynaptic boutons of mammalian, unmyelinated mossy fiber axons in the hippocampus and found to be near the theoretical minimum (1.3-fold excess), making action potential signaling in these axons very efficient[10]. What is unclear is whether this finding is applicable to other mammalian axons or whether action potential efficiency is cell type dependent[11,12]. Furthermore, in both neocortical and mossy fiber axons, the action potential waveform is not constant and depends on the frequency of action potential generation, as well as the membrane potential from which action potentials are initiated[13–16]. Given that differences in the action potential waveform may influence Na^+ excess[11], we hypothesized that action potential metabolic cost is not static and depends on the state of network activity. In addition, it is not well understood how action potential metabolic cost varies across different subcellular compartments of the same neuron.

To address these issues, we investigated the action potential energy budget of cortical layer 5 (L5) pyramidal neurons using direct Na^+ and K^+ current recordings from different subcellular compartments combined with realistic multi-compartmental modeling. We found that action potential efficiency was temporally and spatially heterogeneous. Although dendrites were highly efficient, the sites of action potential initiation in the AIS and the axons were less efficient. Using an *in vivo*–labeled and fully reconstructed thick-tufted cortical L5 pyramidal neuron, we estimated that action potential propagation into the dendrites and the axon consumed ~90% of the total action potential energy budget. In terms of ATP consumption, the total cost per action potential was observed to range from ~480 to ~800×10^6 ATP molecules, depending on cell morphology. Finally, we found that excess axonal Na^+ influx was critical for action potential conduction at high frequencies, revealing a trade-off between energy minimization and conduction reliability.

RESULTS

Location dependence of action potential efficiency

To determine the metabolic cost associated with action potential signaling at different locations in the same neuron, we recorded Na^+ and K^+ currents activated by action potential voltage commands in outside-out patches from the apical dendrites (~170 and ~550 µm

[1]European Neuroscience Institute Göttingen, Göttingen, Germany. [2]Carl Ludwig Institute of Physiology, Medical Faculty, University of Leipzig, Leipzig, Germany. [3]Department of Integrative Neurophysiology, Center for Neurogenomics and Cognitive Research, Neuroscience Campus Amsterdam, VU University Amsterdam, Amsterdam, The Netherlands. [4]Eccles Institute of Neuroscience, The John Curtin School of Medical Research, The Australian National University, Canberra, Australia. [5]Department of Axonal Signaling, Netherlands Institute for Neuroscience, an Institute of the Royal Netherlands Academy of Arts and Sciences, Amsterdam, The Netherlands. Correspondence should be addressed to M.H.P.K. (m.kole@nin.knaw.nl).

Received 27 February; accepted 10 May; published online 3 June 2012; doi:10.1038/nn.3132

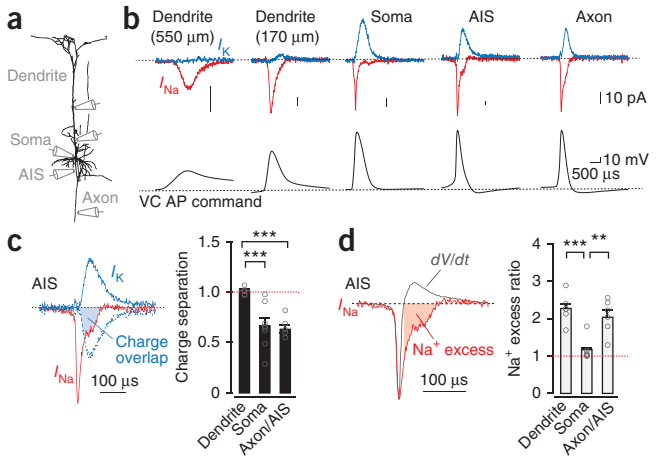

Figure 1 Location dependence of action potential efficiency. (**a**) Illustration of dendritic, somatic, AIS and axonal outside-out patch-clamp recording locations from an *in vitro*–reconstructed thick-tufted L5 pyramidal neuron. (**b**) Pharmacologically isolated Na^+ (red) and K^+ (blue) currents together with voltage-clamp action potential (VC AP) command potentials (black, bottom) at the indicated recording sites. Na^+ and K^+ currents were recorded from difference patches, representing averages of 2–5 recordings. (**c**) Left, AIS action potential waveform evoked Na^+ (red) and K^+ (blue) currents. Scaling as in **b**. The extent of charge overlap is indicated by the filled area (blue; dashed blue line represents inverted K^+ currents). Right, population data of charge separation ratios (individual data, open gray circles). Red dotted line indicates maximally efficient charge separation (1.0). Data are presented as mean ± s.e.m. (**d**) Left, example of AIS action potential capacitive currents (gray) normalized to the Na^+ current peak (red). Filled red area indicates the excess Na^+ influx, following the peak of the action potential ($dV/dt = 0$). Right, population data of the excess ratios for the indicated groups (individual data, open gray circles). Red dotted line indicates maximally efficient Na^+ excess ratio (1.0). Tukey multiple comparison tests, $^{***}P < 0.001$, $^{**}P < 0.01$. Data are presented as mean ± s.e.m.

from the soma), the soma, the AIS and axon cut-endings (up to 300 µm from the soma) of neocortical L5 neurons (**Fig. 1a**). Na^+ and K^+ fluxes were studied by applying an action potential voltage command based on previously recorded action potentials from these sites[13], and ionic currents were pharmacologically isolated in separate voltage-clamp recordings (see Online Methods). We found that the amplitude and kinetics of Na^+ and K^+ currents activated by action potentials were highly location dependent (**Fig. 1b**).

We first evaluated action potential efficiency on the basis of the overlap of Na^+ and K^+ influx during the action potential (**Fig. 1c**). Action potential efficiency was quantified as the ratio of Na^+ influx (charge) that did not overlap with K^+ efflux compared with total Na^+ influx per action potential[10] (**Fig. 1c**). Ratios less than 1 indicate charge overlap, and therefore less efficient action potential generation. Using this measure, we observed significant differences in action potential efficiency at different locations (one-way ANOVA, $P < 0.0001$; **Fig. 1c**). Although charge separation was highly efficient in dendrites (ratio = 1.01 ± 0.02, $n = 6$), a much lower efficiency ratio was observed in the soma and axon (soma, 0.67 ± 0.08, $n = 8$; axon, 0.63 ± 0.03, $n = 8$; Tukey multiple comparison test, $P < 0.001$ for both).

An alternative measure of action potential efficiency is how Na^+ flux compares with the theoretical minimum required to generate the upstroke of the action potential. Action potential efficiency in this manner is quantified[11,17] by taking the ratio of total Na^+ flux (Na^+ current integrated over the entire duration of the action potential) compared with Na^+ flux until the time of the action potential peak ($dV/dt = 0$). Using this metric, ratios greater than 1 indicate excess Na^+ influx, and therefore less efficient action potential generation. As with Na^+ and K^+ charge overlap, the Na^+ excess ratio was location dependent (one-way ANOVA, $P < 0.0002$; **Fig. 1d**). Consistent with previous estimates at the cell body of cortical pyramidal neurons[11], this ratio was close to 1 at the soma (ratio = 1.18 ± 0.13, $n = 6$; **Fig. 1d**). However, Na^+ currents recorded in outside-out patches from axons (AIS or primary axon) were substantially prolonged compared with the first derivative of the action potential waveform (**Fig. 1d**), leading to significantly higher Na^+ excess ratios (ratio = 2.28 ± 0.16, $n = 6$, Tukey multiple comparison test, $P < 0.001$). To determine whether these differences in the Na^+ excess ratio were a result of the action potential waveform or Na^+ channel kinetics, we measured Na^+ current in somatic outside-out patches activated by axonal action potential voltage commands. We found that Na^+ excess ratios were even larger (ratio = 4.5 ± 1.0, $n = 5$, t test, $P < 0.026$ compared to axonal ratio; **Supplementary Fig. 1**), indicating that axonal Na^+ channels inactivate faster than somatic Na^+ channels, but still cannot prevent excess Na^+ influx during the rapid axonal action potential.

The Na^+ excess ratio also exceeded 1 in the dendrites (ratio = 2.04 ± 0.14, $n = 8$, Tukey multiple comparison test, $P < 0.001$). However, this was attributed to a temporal delay in the activation of local ionic currents, as expected for a propagating event in which the rising phase of the action potential waveform is driven by charge flow from more proximal regions[18,19], and was not a result of inefficient action potential generation in dendrites. Together, these data suggest that the efficiency of action potential generation and propagation differs substantially between compartments of single neurons, primarily as a result of the local action potential waveform.

Effect of membrane potential on action potential efficiency

If action potential shape regulates Na^+ excess, then changes in the action potential width would be expected to alter action potential efficiency. In neocortical axons, action potential width is highly dependent on the membrane potential because of its influence on the degree in K^+ channel availability[13,14]. Depolarizations of ~10 mV, as during naturally occurring up states, lead to a ~1.4-fold broadening of the axonal action potential. To determine the effect of membrane potential on axonal action potential efficiency, we compared action potential voltage commands obtained at a depolarized membrane potential (−62 mV, action potential width = 490 µs) with those obtained by action potential voltage commands from the resting membrane potential (−77 mV; **Fig. 2a**). We found that axonal excess Na^+ influx was minimal at depolarized membrane potentials (ratio = 1.1 ± 0.1) compared with the at the resting membrane potential (ratio = 1.8 ± 0.2, paired t test, $P < 0.007$, $n = 4$; **Fig. 2a**,**b**), indicating that action potential generation is more efficient at depolarized membrane potentials.

We also estimated the dependence of axonal action potential efficiency on membrane potential by comparing the overlap of Na^+ influx to K^+ efflux. At the resting membrane potential (−77 mV), the onset of K^+ channel activation during axonal action potentials was delayed by only 73 ± 24 µs compared with Na^+ channel activation, leading to a Na^+/K^+ charge separation ratio of 0.61 ± 0.10 ($n = 4$; **Fig. 2a**,**b**). At depolarized membrane potentials (−62 mV), however, the onset of K^+ channel activation was delayed by 231 ± 13 µs (paired t test, $P < 0.003$, $n = 4$). As a result, the Na^+/K^+ separation ratio was significantly increased (0.86 ± 0.11, paired t test, $P < 0.05$, $n = 4$; **Fig. 2a**,**b**), indicating more efficient action potential generation. In addition, as depolarization leads to inactivation of Na^+ channels, the total Na^+

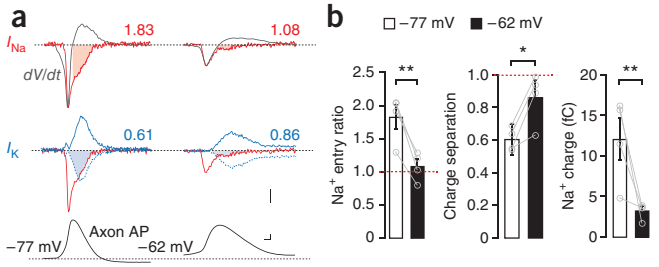

Figure 2 Effect of membrane potential on Na^+ and K^+ flux during axonal action potentials. (**a**) Top, Na^+ currents (red) elicited in axonal outside-out patches during action potential voltage commands (bottom) at the resting potential (left) and depolarized membrane potentials (right). Middle, corresponding K^+ currents (blue), overlaid with the Na^+ currents (red). The extent of charge separation of Na^+ and K^+ currents is indicated by the filled area (blue). Each current represents an average of four paired recordings with both action potential voltage commands (bottom). Scale bars represent 10 pA, 20 mV and 100 µs. Numbers indicate the Na^+ excess ratio (red) or the charge separation ratio (blue). (**b**) Population data of the effect of subthreshold depolarization on the Na^+ entry ratio, Na^+/K^+ charge separation and total Na^+ charge in axonal recordings. Paired *t* tests, $^{**}P < 0.01$, $^{*}P < 0.05$. Data are presented as mean ± s.e.m.

cost per action potential was reduced by 73 ± 0.1% (3.2 ± 0.5 fC at −62 mV, 12.1 ± 2.6 fC at −77 mV; paired *t* test, $P < 0.002$, $n = 4$; **Fig. 2a**,**b**). These data suggest that action potential efficiency and metabolic cost in axons is dynamically dependent on the membrane potential and K^+ channel availability.

Axonal K^+ channels rapidly activate and deactivate

The extent of Na^+/K^+ charge separation during an action potential is determined by the interaction between the speed of Na^+ channel inactivation and K^+ channel activation[10,12,20]. In cortical axons, the primary K^+ channel isoform responsible for repolarizing the action potential is $K_v1.2$, either alone or in combination with $K_v1.1$ (refs. 13,14). Consistent with earlier reports[13,14], application of DTX-I (500 nM, a specific blocker of $K_v1.1$, $K_v1.2$ and $K_v1.6$ channels) blocked 74 ± 1% of the axonal K^+ current evoked by voltage steps (paired *t* test, $P < 0.033$, $n = 6$). Notably, the K^+ currents that were not blocked by DTX-I activated more slowly than the DTX-sensitive current, consistent with DTX-sensitive currents having a primary role in action potential repolarization (control average, 258 ± 23 µs; DTX-I average, 535 ± 32 at +48 mV; paired *t* test, $P < 0.0011$, $n = 6$; **Fig. 3a**). These data suggest that the main K^+ channel involved in the rapid time course of action potential repolarization in neocortical axons is K_v1 (refs. 13,14,21).

Estimating the total energy budget in cortical L5 pyramidal neurons during action potentials requires a detailed compartmental model that accurately reproduces the action potential waveform at different subcellular locations. Thus, we characterized axonal K^+ currents as a first step in the development of an accurate axonal K^+ model based on whole-cell (amplitude range, 1.9–3.8 nA, $n = 17$; **Fig. 3b**) and outside-out voltage-clamp recordings (amplitude range, 0.070–1.3 nA, $n = 8$) from axon cut-ends. Axonal K^+ current activated with a delay, after which it was well fitted with a mono-exponential function with activation time constants ranging from ~1.2 ms to 250 µs for voltages between −42 and +63 mV, respectively (**Fig. 3b**). During action potential–clamp protocols, the activation of K^+ currents had a 10–90% rise time of 150 ± 17 µs ($n = 7$; **Fig. 2a**), which is somewhat faster than K^+ kinetics reported in mossy fibers[22]. K^+ channel deactivation was measured after short depolarizations to +23 mV (**Fig. 3b**). The voltage dependence of activation and deactivation could be approximated by exponential functions with an *e*-fold change in the time constants of activation and deactivation of 40 and 33 mV, respectively (**Fig. 3c**). Steady-state activation and inactivation curves indicated that axonal K^+ channels have a steep voltage dependence of inactivation (−67.9 ± 3.2 mV, slope = 6.3 ± 1.1 mV^{-1}, $n = 4$; **Fig. 3d**), with a substantial non-inactivating component, and shallow voltage dependence of activation (−29.3 ± 1.5 mV, slope = 14.8 ± 0.8 mV^{-1}, $n = 5$). These properties are consistent with those of rapidly activating K_v1-type K^+ channels.

An eight-gate axonal K^+ model predicts a high channel density

We next developed a Hodgkin-Huxley model[18] that captured the experimentally determined voltage dependence and kinetics of axonal K^+ channels on timescales ranging from sub-millisecond (during activation) to several seconds (during slow inactivation). In addition, we compared this Hodgkin-Huxley model to a Zagotta-Hoshi-Aldrich (ZHA) state model[23]. To determine the parameters of the models in an unbiased way, we optimized the models to simultaneously reproduce the recorded activation, deactivation and inactivation currents, as well as the steady-state voltage dependence of activation, inactivation and recovery from inactivation (Online Methods, **Fig. 4a**, **Supplementary Fig. 2** and **Supplementary Table 1**). To test whether these models could describe the K^+ current during action potentials in the AIS, we used action potential voltage commands to simulate the K^+ currents with the different models

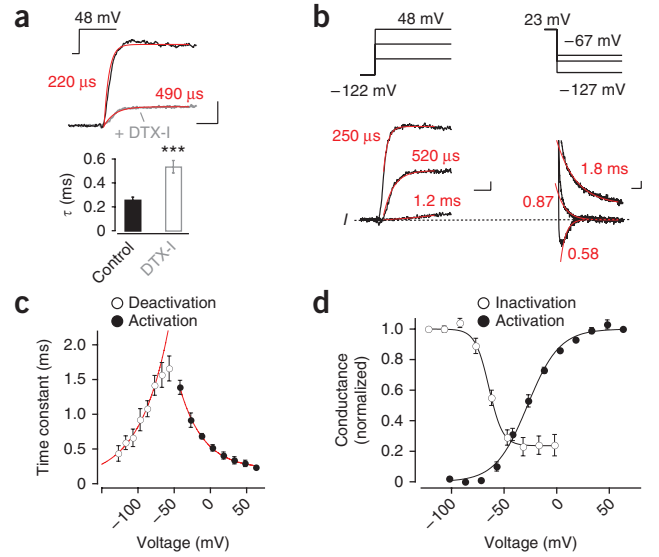

Figure 3 Axonal K^+ channels rapidly activate and deactivate. (**a**) Top, step-induced axonal K^+ currents in whole-cell mode in control (black) and after application of DTX-I (gray, 500 nM). The single exponential fits are overlaid (red) and time constants are indicated. Bottom, population data of the activation time constants showing a significant slowing in response to DTX-I application (paired *t* test $P < 0.001$, $n = 5$). Scale bars represent 0.5 nA and 1 ms. (**b**) Examples of axonal K^+ current activation and deactivation currents (average of four experiments) superimposed with exponential fits (red). The voltage protocols are illustrated above the traces. Scale bars represent 1 ms and 50 pA. (**c**) Time constants of exponential fits to activation (filled) and deactivation (open circles) superimposed with exponential fits (red, 40.0 and 32.7 mV per *e*-fold change in activation and inactivation rate constants). Data are presented as mean ± s.e.m. (**d**) Steady-state activation (closed circles) and inactivation (open circles). Shown are average data fit with a Boltzman equation yielding a half-maximum activation voltage of −30.1 mV and half-maximum inactivation voltage of −67.9 mV. Data are presented as mean ± s.e.m.

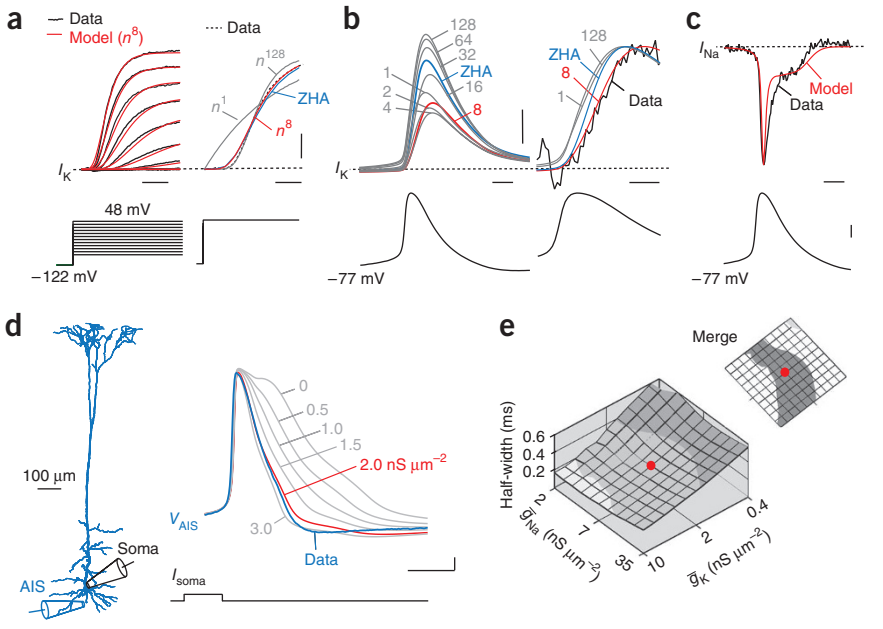

Figure 4 An eight-gate axonal K^+ model predicts a high channel density. (**a**) Left, steady-state activation currents (black) superimposed with predictions of a Hodgkin-Huxley model (red) with eight activation gates (n^8). The voltage-step command protocol is indicated below. Right, expanded data overlaid with 1-, 8- and 128-gate Hodgkin-Huxley models, as well as the ZHA state model (blue). Scale bars represent 500 pA (top), 500 µs (left) and 200 µs (right). (**b**) Left, simulated K^+ current evoked by AIS action potential command potential with Hodgkin-Huxley models with different numbers of activation gates (1–128) and ZHA model (blue). Scale bar represents 2 mA cm^{-2}. Right, expanded and normalized currents. Note the good prediction of the activation delay and rising phase of the experimental data (black) with eight Hodgkin-Huxley gates (red). Scale bars represent 2 mA cm^{-2} (top), 200 (left) and 100 µs (right). (**c**) Simulated Na^+ current based on an eight-state model[24] superimposed on the experimentally recorded action potential evoked Na^+ current. Scale bars represent 100 µs (top) and 20 mV (bottom). (**d**) Left, morphology of a L5 model neuron. Right, overlay of simulated (gray) and experimentally recorded AIS action potential (blue) showing that models with $\bar{g}_K$ of 2,000 pS µm^{-2} in the distal AIS best describe the action potential repolarization. Scale bars represent 500 µs and 10 mV. Bottom, somatic current injection is indicated (3 ns, 1 nA). (**e**) Top, systematic evaluation of the half-width of the AIS action potential in models with different $\bar{g}_{Na}$ and $\bar{g}_K$. Corresponding analysis of additional action potential parameters (**Supplementary Fig. 3**) revealed the best-fit parameters $\bar{g}_{Na}$ = 7,000 and $\bar{g}_K$ = 2,000 pS µm^{-2} (red point). Inset, same plot shown as viewed from above with the darker area indicating values that fall in the target range (half-width 250–400 µs).

(**Fig. 4b**). We found that axonal K^+ currents activated by conventional step voltage commands, as well as action potential waveforms, were best described by a n^8 Hodgkin-Huxley model (**Fig. 4a**,**b** and **Supplementary Fig. 2**). To simulate Na^+ currents, we took advantage of a recently established eight-state Na^+ channel model, based on detailed analysis of Na^+ currents in hippocampal granule cell axons[24]. This Na^+ channel model adequately described action potential–evoked Na^+ currents and Na^+ excess during action potential repolarization (**Fig. 4c**).

We then used these Na^+ and K^+ channel models to replicate action potential initiation in a model based on the reconstructed morphology of a cortical L5 pyramidal neuron from which action potentials were recorded simultaneously at the soma and AIS (44 µm from the soma in the cut-end; **Fig. 4d**). AIS K^+ and Na^+ peak conductance densities ($\bar{g}_K$ and $\bar{g}_{Na}$, respectively) were estimated by comparing experimentally recorded action potentials with those predicted by the model (**Fig. 4d** and **Supplementary Fig. 3**). These simulations showed that $\bar{g}_K$ needed to be as high as ~2,000 pS µm^{-2} in the distal end of the AIS to reproduce the half width of action potentials in the AIS, whereas $\bar{g}_{Na}$ needed to be as high as 7,000 pS µm^{-2} to reproduce the amplitude and rate of rise of action potentials in the AIS (**Fig. 4d**,**e**). Models with these densities reproduced a wide range of action potential parameters, including action potential peak, rate of rise and threshold behavior (**Supplementary Fig. 3**). In addition, taking all action potential properties into account, the required $\bar{g}_{Na}$ appeared to be relatively independent of the modeled Na^+ kinetics (**Supplementary Fig. 4**).

K^+ channel inactivation regulates Na^+/K^+ charge separation

We next used our model to investigate how changes in membrane potential can influence action potential metabolic cost, as we observed experimentally (**Fig. 2**). Action potentials in these simulations were elicited by somatic current injection after long (10 s) depolarizations in a L5 model neuron that included the primary axon (**Fig. 5a**). Depolarization of the membrane potential by approximately 10 mV (from −77 to −68 mV) led to inactivation of axonal K^+ channels by 65% and increased axonal action potential width approximately 1.3-fold (**Fig. 5a**), similar to that observed experimentally[13,25]. These changes were associated with inactivation of Na^+ channels by approximately 33% and an increase in the charge separation ratio by 23% (from 0.44 to 0.54; **Fig. 5b**). To test whether this observed increase in action potential efficiency at depolarized potentials also occurs during naturalistic patterns of activity, we investigated action potential initiation during synaptic activity in the model. Synapses were randomly added to ten locations in the basal dendrites and activated with stochastic Poisson-like firing patterns (**Fig. 5c**). Integration of these synaptic inputs caused a subthreshold depolarization of approximately 5 mV, inactivating axonal $\bar{g}_K$ by 48%, leading to 1.2-fold action potential broadening and ultimately increasing charge separation by 14% (from 0.44 to 0.50).

To gain more insight into the contribution of Na^+ and K^+ channel gating to regulation of axonal action potential metabolic cost, we evaluated charge separation in models with different degrees of Na^+ and K^+ channel inactivation (**Fig. 5d**). The systematic analysis revealed that inactivation of K^+ channels has a stronger effect on charge separation than inactivation of Na^+ channels. This can be explained by the fact that action potential half width is critical for determining charge separation[11] (**Figs. 1** and **2**) and that Na^+ channel availability has a large effect on action potential amplitude, but only a small effect on action potential half width (**Supplementary Fig. 3**). In summary, we found that the charge separation during axonal action potential generation was primarily regulated by the degree of steady-state K^+ channel inactivation, which is determined by the functional state of the network in which the neuron is embedded.

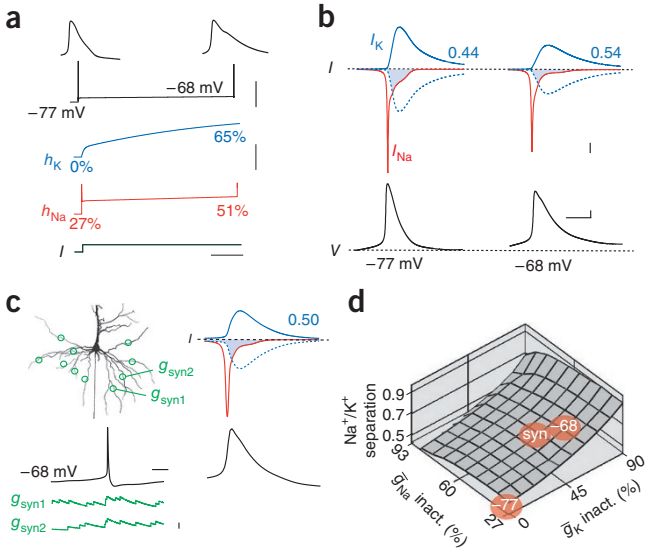

Figure 5 K^+ channel inactivation regulates Na^+/K^+ charge separation. (**a**) Steady current injection for 10 s (bottom) induced a subthreshold depolarization from –77 to –68 mV. Additional current injections elicited action potentials before and at the end of the 10-s depolarization. The time course of inactivation of K^+ and of Na^+ channels is shown in blue (h_K) and red (h_{Na}), respectively. Scale bars represent 50 mV, 50% and 2 s. (**b**) Top, corresponding AIS K^+ (blue) and Na^+ (red) currents during action potentials (below) at the resting membrane potential of –77 mV (left) and after subthreshold depolarization (10 s) to –68 mV. The overlap of the Na^+ and the inverted K^+ current (dashed blue) is indicated (filled blue). Scale bars represent 1 mA cm^{-2}, 10 mV and 500 µs. (**c**) Top left, ten synapses (green circles) were added to the basal dendrites and activated with random Poisson firing. Bottom left, voltage trace of an action potential elicited by the synaptic input and two examples of corresponding synaptic conductances (green). Scale bars represent 10 ms and 2 nS. Right, axonal Na^+ (red) and K^+ (blue) currents underlying the action potential evoked by synaptic input together with action potential waveform (below). Same scaling as in **b**. (**d**) Systematic evaluation of the AIS charge separation evaluated with different degrees of Na^+ and K^+ channel inactivation. The development of the charge separation during subthreshold depolarization from –77 to –68 mV (**a**,**b**) and during synaptic input (syn, green, **c**) are superimposed on the graph.

Action potential metabolic cost is spatially heterogeneous

We found that action potential efficiency differs substantially between subcellular compartments in the same neuron (**Fig. 1**), which complicates estimates of action potential metabolic cost based on a single efficiency value[1,26]. We therefore decided to determine the total energy budget in cortical L5 neuron models by analyzing Na^+ influx into each segment separately (**Fig. 6**). The experimentally determined Na^+/K^+ charge overlap (**Fig. 1b**) was well captured in the model (**Fig. 6a**,**b**). Although the main primary apical trunk until the first branch point was characterized by highly efficient Na^+/K^+ charge separation (ratio = ~0.85), Na^+/K^+ charge separation was least at the distal AIS (ratio = 0.36; **Fig. 6a**,**b** and **Supplementary Fig. 5**).

To obtain a quantitative estimate of the total energy budget underlying action potential initiation and propagation in L5 pyramidal neurons, we used models obtained from cortical L5 neurons recorded *in vitro* and *in vivo*, of which the latter included the complete

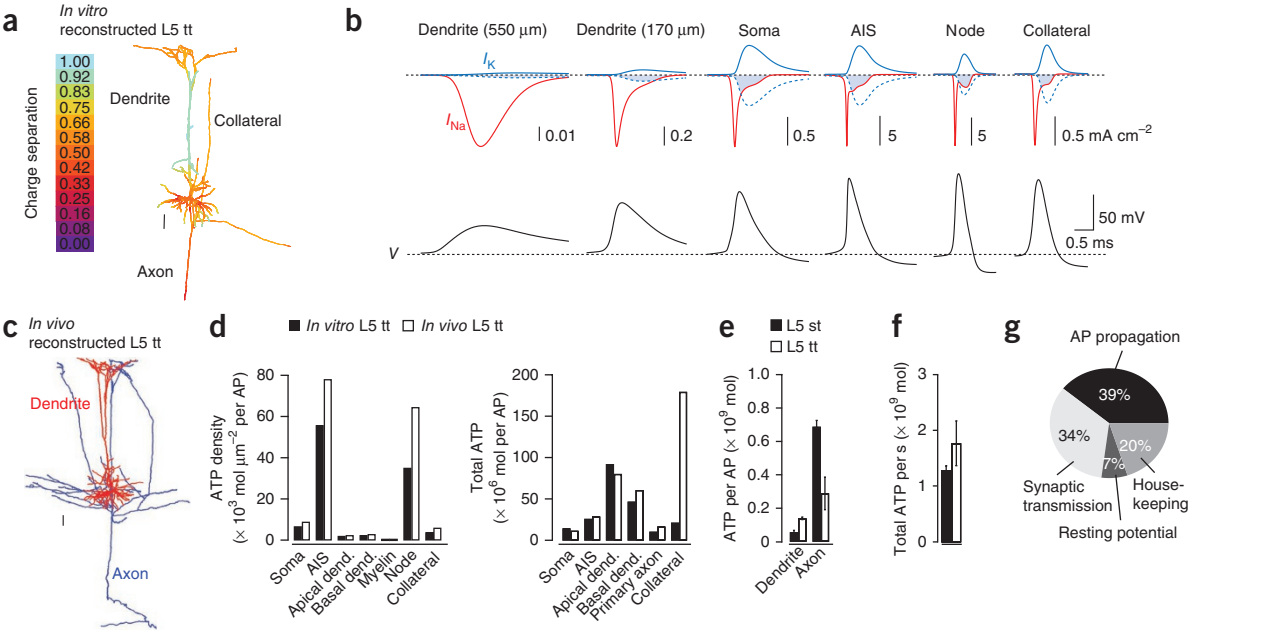

Figure 6 Action potential metabolic cost is spatially heterogeneous. (**a**) Color-coded space plot of the *in vitro* biocytin-filled thick-tufted (tt) L5 neuron. Colors indicate the Na^+/K^+ charge separation ratio (0–1) during propagation of a single action potential. Scale bar represents 100 µm. (**b**) Local Na^+ (red) and K^+ (blue) currents activated during the back- and forward-propagating action potential in the model shown in **a**. Charge overlap is indicated with blue areas. Note the similarities to experimentally recorded locations in **Figure 1b**. (**c**) Semi-coronal projection of an *in vivo* biocytin-filled thick-tufted L5 neuron used for simulations. Note the extensive axon collaterals (blue) compared with dendrites (red). Scale bar represents 100 µm. (**d**) Bar plots of the ATP per unit membrane area (left) and total ATP consumption (right) per subcellular location and per action potential comparing the *in vitro* (closed) and *in vivo* (open) reconstructed neuron. (**e**) ATP per action potential for the cumulative dendritic and axonal areas from thick-tufted and slender-tufted (st) *in vivo* labeled L5 neurons ($n = 3$ each, $P < 0.05$ for both dendrite and axon). (**f**) Rate of ATP consumption in thick- and slender-tufted L5 neurons. Note that both neurons consume ATP at an approximately similar rate ($n = 3$, $P > 0.09$). (**g**) Pie chart of the proportion of ATP usage for action potential generation in thick-tufted L5 neurons, comparing housekeeping, resting potential, action potential propagation and synaptic transmission costs.

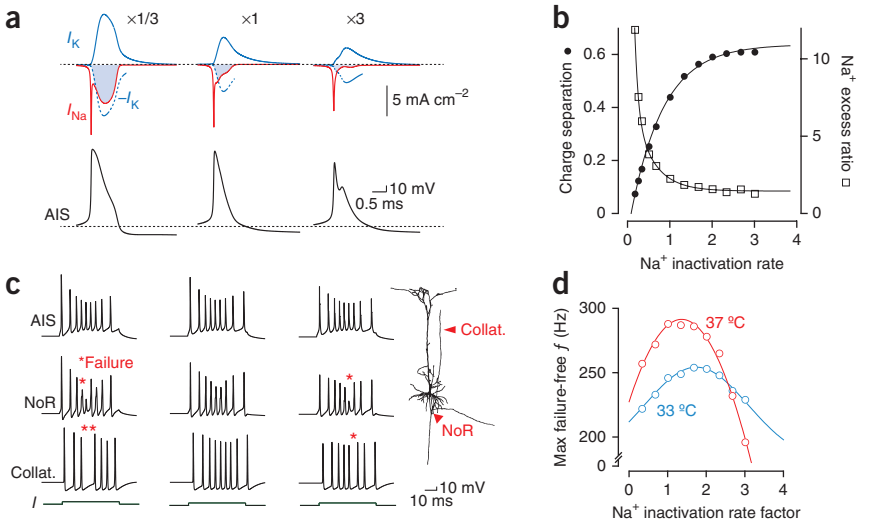

Figure 7 Axonal Na^+ channel inactivation is optimal for high-frequency action potentials. (**a**) Top, examples of simulated Na^+ (red) and K^+ (blue) currents during AIS action potentials with reduced (×1/3), control (×1) and increased (×3) Na^+ inactivation rates in the axon. The resulting Na^+/K^+ charge overlap is indicated (blue). Bottom, AIS action potentials associated to the different Na^+ inactivation rates. (**b**) Relationship between the scaling factor of the inactivation rate versus Na^+/K^+ charge separation (closed circles) and Na^+ excess ratio (open squares) at 33 °C. Solid lines represent double exponential fits to the data. (**c**) High-frequency action potential burst for the different Na^+ inactivation rates as in **a**. Traces show the action potentials in the AIS, the first NoR and the collaterals as indicated by the red arrowheads. Note the failures in propagation for the high-frequency action potentials in a burst (red asterisks). Current injection amplitudes were 2.3, 1.2 and 0.9 nA. (**d**) Scaling factor of Na^+ inactivation rates versus the maximum possible failure-free firing rate (f) for 33 °C (blue) and 37 °C (red) simulation temperature (blue and red lines, Gaussian functions with peaks at 1.36 and 1.16, respectively).

intracortical axonal collateral arborization[27] (**Fig. 6c**). To estimate ATP consumption, we assumed three Na^+ ions were extruded per ATP molecule[1]. We found that, although the ATP requirement in apical dendritic compartments was small per unit area compared with the AIS, about fivefold more ATP molecules were required for action potential backpropagation into dendrites (basal and apical) than for action potential initiation in the AIS (**Fig. 6d**). Forward propagation of action potentials through unmyelinated axon collaterals also consumed large amounts of ATP, although action potential propagation through the myelinated primary axon was the least expensive part of action potential signaling in L5 neurons. On the basis of these estimates, the cumulative metabolic cost for all compartments revealed that the total energy consumption per action potential was 202 and 377 × 10^6 ATP molecules in the *in vitro* and *in vivo* thick-tufted L5 neuron, respectively. These values varied by less than ±10% for a range of realistic dendritic and axonal Na^+ channel densities (**Supplementary Fig. 5e**,**f**).

We next compared ATP consumption between the two main classes of L5 pyramidal neurons: thick-tufted L5 neurons characterized by an elaborate dendritic tuft with typically few intracortical axonal projections and slender-tufted L5 neurons characterized by relatively simple apical tuft branching, but intricate long-range axonal projections leaving the principal column[27]. Using *in vivo* L5 reconstructions, we found that the ATP consumption per action potential was higher in slender-tufted than in thick-tufted L5 neurons (800 ± 50 × 10^6 versus 480 ± 100 × 10^6 ATP, $n = 3$ each, $P < 0.007$), primarily because of the larger axonal arborization (**Fig. 6e**). However, taking the lower average action potential firing rate in these neurons into account (slender-tufted, 1.64 Hz; thick-tufted, 3.77 Hz)[28,29], the rate of ATP consumption was slightly lower in slender L5 neurons (**Fig. 6f**). To understand how the cost of action potentials compares with other cellular processes related to action potential firing[1], we calculated the cost of maintaining the resting membrane potential for 1 s and estimated the downstream cost for synaptic transmission in the axonal arborization of thick-tufted L5 neurons (Online Methods). These calculations revealed that action potential initiation and propagation represents the highest metabolic cost (39%), followed by synaptic transmission (34%; **Fig. 6g**).

Na^+ inactivation is optimal for high-frequency firing

Excess Na^+ influx during action potential generation has previously been noted in a range of neuron cell types that generate high-frequency action potential firing or complex action potential bursts, including cerebellar Purkinje neurons, GABAergic interneurons and vestibular neurons[11,30,31]. Given that cortical L5 axons are also able to generate high-frequency action potential bursts at up to 400 Hz[32,33], we hypothesized that the high metabolic cost of incomplete Na^+ channel inactivation during action potential initiation may trade-off metabolic efficiency for the capacity to generate high-frequency burst firing. To test this hypothesis, we manipulated the inactivation kinetics of axonal Na^+ channels in our model (**Fig. 7a**). Increasing the speed of Na^+ channel inactivation (×3) reduced the Na^+ excess ratio to 1.3 (compared to 2.8), indicating that action potentials were more efficient, whereas slowing Na^+ channel inactivation (×1/3) increased the Na^+ excess ratio to 6.0, indicating that efficiency was reduced (**Fig. 7a**,**b**). Speeding up the rate of inactivation for a given Na^+ channel density also led to a reduction in action potential amplitude (**Fig. 7a**).

Finally, we investigated the effect of the rate of Na^+ channel inactivation on the propagation of high-frequency action potential trains (**Fig. 7c**). High-frequency bursts in the control condition consisted of eight action potentials evoked at a maximum frequency of 245 Hz (33 °C). At this frequency, both speeding up and slowing down axonal Na^+ channel inactivation led to failure of action potentials propagating down the axon (**Fig. 7c**). In particular at a nominal temperature of 37 °C, the highest firing frequency without propagation failure (296 Hz) occurred when the Na^+ channel inactivation rate was close to that observed experimentally (scaling factor = 1.16; **Fig. 7d**). Together, these simulations suggest that the observed excess Na^+ influx in myelinated axons is optimized for high-frequency firing despite the additional metabolic cost.

DISCUSSION

Our study is, to the best of our knowledge, the first investigation of the state- and location-dependence of action potential efficiency and action potential metabolic cost in single neurons. Metabolic efficiency was found to depend on the membrane potential as well as

the subcellular compartment. In neocortical axons, Na^+ excess during action potentials was observed to be ~2.1-fold greater than the theoretical minimum (**Fig. 1**). Although substantially more efficient than the fourfold Na^+ excess measured in the frog NoR and squid axon[8,9,18], action potential initiation and propagation in these axons is less efficient than recent observations in unmyelinated hippocampal mossy fiber axons (1.2–1.3)[10,24]. The high ionic efficiency of mossy fiber axons, which have similar action potential half-widths as action potentials in the L5 axon, may reflect specialized Na^+ channel inactivation kinetics or slower and delayed activation of K^+ channels in these axons[22,24,34]. Indeed, we found that the onset of K^+ efflux in neocortical axons started rapidly and occurred during the action potential rising phase, ~70 µs after the onset of Na^+ influx (**Figs. 1** and **2**). This delay is about ~30 µs shorter than that observed in mossy fibers[22]. Rapid activation of K^+ currents will limit the completeness of Na^+ channel inactivation and, as a consequence, Na^+ influx continues for hundreds of microseconds during the falling phase of the action potential. These cell type–specific K^+ channel gating properties likely reflect differences in the expression of specific K^+ channel isoforms mediating the outward K^+ current in axons. Consistent with this idea, the K^+ current during the action potential repolarization is dominated by K_v1 in neocortical axons[13,14], whereas K_v3 channels predominate action potential repolarization in mossy fibers[22]. These observations indicate that differences in K^+ channel expression and subunit composition have a large effect on the metabolic cost of action potential generation and propagation in neurons.

By analyzing native K^+ channels in the AIS of L5 pyramidal neurons using Hodgkin-Huxley[18] and state models[23], our data indicate that two independent activation gates are required for each of the four subunits (**Supplementary Fig. 2e**)[23,35,36]. The inactivation kinetics appears to reflect heterogeneous channel populations with different inactivation kinetics rather than two inactivation gates per channel. There is considerable molecular evidence supporting this hypothesis, as K_v1 channels are known to assemble as heterotetrameric complexes with subunits of diverse kinetic properties[37,38]. High-power immunofluorescence of the cortical pyramidal AIS has demonstrated the presence of densely clustered and colocalized $K_v1.1$, $K_v1.2$ and $K_v1.4$ α-subunits together with auxiliary $K_v1.2$ β-subunits[39–42].

On the basis of Na^+/K^+ charge separation, we can conclude that action potentials in both the soma and axon of cortical L5 pyramidal neurons were inefficient (**Fig. 1c**). In contrast, using Na^+ excess as a measure of efficiency suggested that somatic action potential generation was quite efficient (**Fig. 1d**), consistent with previous estimates in acutely dissociated cortical pyramidal neurons[11]. Differences between both measures became even more apparent at the distal dendrites of L5 pyramidal neurons, where action potential propagation was very efficient on the basis of Na^+/K^+ charge separation (ratio = 1.01; **Fig. 1**), but inefficient on the basis of the Na^+ excess (ratio = 2.04). However, the use of the Na^+ excess ratio as a means to estimate action potential efficiency is complicated by the fact that this measure does not take into account the amplitude of Na^+ influx, just its time course. Na^+ excess ratio measures therefore cannot be used when a substantial component of the action potential upstroke derives from passive charging, as occurs at the soma during invasion of the AIS spike and in the dendrites during backpropagation of the action potential.

What is the global ATP consumption of L5 pyramidal neurons? Given that during passive whisker deflection L5 neurons generate about 60% of all sensory-related action potentials in a cortical column[29], they must be important for the overall gray matter energy budget. Using models of L5 pyramidal neurons from *in vivo* recordings, containing the complete three-dimensional axonal and dendritic tree, we directly calculated that the total quantity of ATP molecules required to restore the Na^+ and K^+ gradient after one action potential is between ~480 and ~800 × 10^6 ATP molecules for average thick- and slender-tufted L5 neurons, respectively (**Fig. 6**). For thick-tufted L5 neurons, this is close to the previous estimate of ~400 × 10^6 (ref 1), which was, however, based on the smaller layer 2/3–type pyramidal neuron. A cell type–dependent analysis of metabolic cost has not yet been carried out. The experimentally measured depolarization-induced reduction in action potential cost in the proximal axons (**Fig. 2**), as would be expected to occur during up states, is likely to have only a small effect on the global metabolic cost (~6% reduction per action potential). When comparing the energetic costs for other cellular processes in L5 pyramidal neurons, we found that action potential initiation and propagation in the thick-tufted cell type accounts for 39% of total energy consumption, slightly more than synaptic transmission (34%). This finding indicates that the general notion that synapses are the dominant component in the neural costs in gray matter[10,26] does not hold for the large L5 pyramidal neurons.

Why is action potential conduction in axons of L5 neurons inefficient? Excess Na^+ in the axon may be involved in supporting high-frequency signaling in the axon. Selectively improving the metabolic efficiency in the axon by speeding up the rate of axonal Na^+ channel inactivation led to action potential propagation failure at high frequencies. This observation is best explained by a frequency-dependent reduction in Na^+ channel availability in the AIS (**Fig. 7**), which leads to insufficient charging of the membrane to support action potential initiation and re-initiation at nodes at high frequencies. Our results are consistent with experimental and theoretical findings that Na^+ influx during action potentials in fast-spiking neurons is larger than the theoretical minimum[11,12]. Action potential failure at high frequencies occurs at the AIS and the first NoR, where a high Na^+ channel density is critical for action potential initiation and charging of axon collaterals, but at the same time is under the influence of the steady-state inactivation via somatic depolarization (**Fig. 7**). We suggest that the evolutionary pressure on Na^+ channel inactivation kinetics in myelinated cortical axons favors reliability of action potential conduction rather than minimizing metabolic cost.

Various elements of the neocortical membrane excitability, other than ionic costs, are likely to have evolved as a consequence of the selective pressures to reduce excess energy expenditure[1,6,43]. For example, it has been hypothesized that the observed sparse action potential firing rates in cortical networks *in vivo* are close to the predicted value to maximize representational capacity of spiking and minimize metabolic cost[1,6]. Furthermore, combined encoding schemes using analog and binary signals in neocortical glutamatergic axons might increase the capacity of information transfer while reducing the local ATP cost of action potential generation[13,25,44]. Finally, the evolution of myelin in neural circuits markedly minimizes the membrane capacitance that has to be charged, potentially further reducing metabolic cost. However, a recent study indicated that, when taking into account the additional cost for producing myelin and maintaining the resting potential of oligodendrocytes, myelination might not save energy overeall[26]. Instead, constraints on brain size and rapid information processing in large nervous systems is likely to be a more important constraint than metabolic cost alone[26,45].

Consistent with these ideas, our findings, based on a bottom-up approach combining direct biophysical recordings and morphology-based computational modeling, indicate that Na^+ inactivation kinetics in cortical axons is optimized for conduction of high-frequency

signals rather than metabolic efficiency. We found that the efficiency, as well as the local metabolic cost, differed substantially between neuronal compartments. Together, these data suggest that the biophysical properties and membrane densities of voltage-gated Na^+ and K^+ channels in cortical neurons primarily reflect the functional requirements of different subcellular compartments rather than minimization of metabolic cost alone.

METHODS

Methods and any associated references are available in the online version of the paper.

Note: Supplementary information is available in the online version of the paper.

ACKNOWLEDGMENTS

The research leading to these results has received funding from the European Research Council under the European Community's Seventh Framework Program (FP7/2007–2013)/ERC Grant agreement n° P261114 and from the Australian National Health and Medical Research Council (NHMRC) Project Grant n° 525437 to M.H.P.K. S.H. received funding from the Heisenberg Program of the German Research Foundation (HA 6386/1-1 and 2-1). The authors are grateful to Henrik Alle and Christoph Schmidt-Hieber for discussions on earlier versions of this manuscript.

AUTHOR CONTRIBUTIONS

S.H. and M.H.P.K. designed and conducted the experiments and analyzed data. C.P.J.d.K. provided the *in vivo* reconstructions. S.H., C.P.J.d.K., G.J.S. and M.H.P.K. wrote the paper.

COMPETING FINANCIAL INTERESTS

The authors declare no competing financial interests.

Published online at http://www.nature.com/doifinder/10.1038/nn.3132.
Reprints and permissions information is available online at http://www.nature.com/reprints/index.html.

1. Attwell, D. & Laughlin, S.B. An energy budget for signaling in the grey matter of the brain. *J. Cereb. Blood Flow Metab.* **21**, 1133–1145 (2001).
2. Aiello, L. & Wheeler, P. The expensive-tissue hypothesis: the brain and the digestive system in human and primate evolution. *Curr. Anthropol.* **36**, 199–221 (1995).
3. Crotty, P., Sangrey, T. & Levy, W.B. Metabolic energy cost of action potential velocity. *J. Neurophysiol.* **96**, 1237–1246 (2006).
4. Herculano-Houzel, S. Scaling of brain metabolism with a fixed energy budget per neuron: implications for neuronal activity, plasticity and evolution. *PLoS ONE* **6**, e17514 (2011).
5. Hodgkin, A. The optimum density of sodium channels in an unmyelinated nerve. *Phil. Trans. R. Soc. Lond. B* **270**, 297–300 (1975).
6. Lennie, P. The cost of cortical computation. *Curr. Biol.* **13**, 493–497 (2003).
7. Levy, W.B. & Baxter, R.A. Energy efficient neural codes. *Neural Comput.* **8**, 531–543 (1996).
8. de Haas, V. & Vogel, W. Sodium and potassium currents recorded during an action potential. *Eur. Biophys. J.* **17**, 49–51 (1989).
9. Frankenhaeuser, B. & Huxley, A.F. The action potential in the myelinated nerve fiber of *Xenopus laevis* as computed on the basis of voltage clamp data. *J. Physiol. (Lond.)* **171**, 302–315 (1964).
10. Alle, H., Roth, A. & Geiger, J.R.P. Energy-efficient action potentials in hippocampal mossy fibers. *Science* **325**, 1405–1408 (2009).
11. Carter, B.C. & Bean, B.P. Sodium entry during action potentials of mammalian neurons: incomplete inactivation and reduced metabolic efficiency in fast-spiking neurons. *Neuron* **64**, 898–909 (2009).
12. Sengupta, B., Stemmler, M., Laughlin, S.B. & Niven, J.E. Action potential energy efficiency varies among neuron types in vertebrates and invertebrates. *PLOS Comput. Biol.* **6**, e1000840 (2010).
13. Kole, M.H.P., Letzkus, J. & Stuart, G. Axon initial segment K_v1 channels control axonal action potential waveform and synaptic efficacy. *Neuron* **55**, 633–647 (2007).
14. Shu, Y., Yu, Y., Yang, J. & McCormick, D.A. Selective control of cortical axonal spikes by a slowly inactivating K^+ current. *Proc. Natl. Acad. Sci. USA* **104**, 11453–11458 (2007).
15. Geiger, J.R.P. & Jonas, P. Dynamic control of presynaptic Ca^{2+} inflow by fast-inactivating K^+ channels in hippocampal mossy fiber boutons. *Neuron* **28**, 927–939 (2000).
16. Kole, M.H. & Stuart, G.J. Signal processing in the axon initial segment. *Neuron* **73**, 235–247 (2012).
17. Carter, B.C. & Bean, B.P. Incomplete inactivation and rapid recovery of voltage-dependent sodium channels during high-frequency firing in cerebellar Purkinje neurons. *J. Neurophysiol.* **105**, 860–871 (2011).
18. Hodgkin, A.L. & Huxley, A.F. A quantitative description of membrane current and its application to conduction and excitation in nerve. *J. Physiol. (Lond.)* **117**, 500–544 (1952).
19. Cole, K.S. & Curtis, H.J. Electric impedance of the squid giant axon during activity. *J. Gen. Physiol.* **22**, 649–670 (1939).
20. Hasenstaub, A., Otte, S., Callaway, E. & Sejnowski, T.J. Metabolic cost as a unifying principle governing neuronal biophysics. *Proc. Natl. Acad. Sci. USA* **107**, 12329–12334 (2010).
21. Lorincz, A. & Nusser, Z. Molecular identity of dendritic voltage-gated sodium channels. *Science* **328**, 906–909 (2010).
22. Alle, H., Kubota, H. & Geiger, J.R. Sparse, but highly efficient, K_v3 outpace BKCa channels in action potential repolarization at hippocampal mossy fiber boutons. *J. Neurosci.* **31**, 8001–8012 (2011).
23. Zagotta, W.N., Hoshi, T. & Aldrich, R.W. Shaker potassium channel gating. III. Evaluation of kinetic models for activation. *J. Gen. Physiol.* **103**, 321–362 (1994).
24. Schmidt-Hieber, C. & Bischofberger, J. Fast sodium channel gating supports localized and efficient axonal action potential initiation. *J. Neurosci.* **30**, 10233–10242 (2010).
25. Shu, Y., Hasenstaub, A., Duque, A., Yu, Y. & McCormick, D.A. Modulation of intracortical synaptic potentials by presynaptic somatic membrane potential. *Nature* **441**, 761–765 (2006).
26. Harris, J.J. & Attwell, D. The energetics of CNS white matter. *J. Neurosci.* **32**, 356–371 (2012).
27. Oberlaender, M. *et al.* Three-dimensional axon morphologies of individual layer 5 neurons indicate cell type–specific intracortical pathways for whisker motion and touch. *Proc. Natl. Acad. Sci. USA* **108**, 4188–4193 (2011).
28. Oberlaender, M. *et al.* Cell type–specific three-dimensional structure of thalamocortical circuits in a column of rat vibrissal cortex. *Cereb. Cortex* (2011).
29. de Kock, C.P. & Sakmann, B. High frequency action potential bursts (>100 Hz) in L2/3 and L5B thick tufted neurons in anaesthetized and awake rat primary somatosensory cortex. *J. Physiol. (Lond.)* **586**, 3353–3364 (2008).
30. Raman, I.M. & Bean, B.P. Resurgent sodium current and action potential formation in dissociated cerebellar Purkinje neurons. *J. Neurosci.* **17**, 4517–4526 (1997).
31. Gittis, A.H., Moghadam, S.H. & du Lac, S. Mechanisms of sustained high firing rates in two classes of vestibular nucleus neurons: differential contributions of resurgent Na, K_v3, and BK currents. *J. Neurophysiol.* **104**, 1625–1634 (2010).
32. Kole, M.H.P. First node of ranvier facilitates high-frequency burst encoding. *Neuron* **71**, 671–682 (2011).
33. Popovic, M.A., Foust, A.J., Mccormick, D.A. & Zecevic, D. The spatio-temporal characteristics of action potential initiation in layer 5 pyramidal neurons: a voltage-imaging study. *J. Physiol. (Lond.)* **589**, 4167–4187 (2011).
34. Engel, D. & Jonas, P. Presynaptic action potential amplification by voltage-gated Na^+ channels in hippocampal mossy fiber boutons. *Neuron* **45**, 405–417 (2005).
35. Schoppa, N.E. & Sigworth, F.J. Activation of Shaker potassium channels. III. An activation gating model for wild-type and V2 mutant channels. *J. Gen. Physiol.* **111**, 313–342 (1998).
36. Yellen, G. The voltage-gated potassium channels and their relatives. *Nature* **419**, 35–42 (2002).
37. Stühmer, W. *et al.* Molecular basis of functional diversity of voltage-gated potassium channels in mammalian brain. *EMBO J.* **8**, 3235–3244 (1989).
38. Hopkins, W.F. Toxin and subunit specificity of blocking affinity of three peptide toxins for heteromultimeric, voltage-gated potassium channels expressed in *Xenopus* oocytes. *J. Pharmacol. Exp. Ther.* **285**, 1051–1060 (1998).
39. Ogawa, Y. *et al.* Postsynaptic density 93 clusters K_v1 channels at axon initial segments independently of Caspr2. *J. Neurosci.* **28**, 5731–5739 (2008).
40. Rhodes, K.J. *et al.* Association and colocalization of the $K_v$beta1 and $K_v$beta2 beta-subunits with K_v1 alpha-subunits in mammalian brain K^+ channel complexes. *J. Neurosci.* **17**, 8246–8258 (1997).
41. Wang, H., Kunkel, D.D., Schwartzkroin, P.A. & Tempel, B.L. Localization of $K_v1.1$ and $K_v1.2$, two K channel proteins, to synaptic terminals, somata, and dendrites in the mouse brain. *J. Neurosci.* **14**, 4588–4599 (1994).
42. Lorincz, A. & Nusser, Z. Cell type–dependent molecular composition of the axon initial segment. *J. Neurosci.* **28**, 14329–14340 (2008).
43. Niven, J.E. Energy limitation as a selective pressure on the evolution of sensory systems. *J. Exp. Biol.* **211**, 1792–1804 (2008).
44. Juusola, M., Robinson, H.P.C. & De Polavieja, G.G. Coding with spike shapes and graded potentials in cortical networks. *Bioessays* **29**, 178–187 (2007).
45. Wang, S.S.-H. *et al.* Functional trade-offs in white matter axonal scaling. *J. Neurosci.* **28**, 4047–4056 (2008).

ONLINE METHODS

Electrophysiological recordings. All experiments complied with guidelines of the animal ethics committee of the Australian National University and the institutional animal care and use committee of the Royal Netherlands Academy of Arts and Sciences. Acute parasagittal cortical brain slices (300 µm) of male Wistar rats (3–5 weeks of age) were prepared following procedures described previously[46]. Slices were perfused with oxygenated (95% O_2, 5% CO_2) artificial cerebrospinal fluid consisting of 125 mM NaCl, 25 mM $NaHCO_3$, 3 mM KCl, 1.25 mM NaH_2PO_4, 25 mM glucose, 2 mM $CaCl_2$ and 1 mM $MgCl_2$. Patch pipettes had an open tip resistance of 4–6 MΩ and filled with 130 mM potassium gluconate (or potassium methylsulfate), 10 mM KCl, 10 mM HEPES, 10 mM sodium phosphocreatine, 4 mM Mg^{2+}-ATP and 0.3 mM Na^+-GTP (pH 7.3, 285 mOsm). Whole-cell and outside-out voltage-clamp recordings were made from dendrites, soma, cut-ends of the AIS and distal axon (>300 µm distal of the soma) of visually identified thick-tufted L5 neurons. Seal resistances were always >1 GΩ. Voltage-clamp recordings were made with an Axopatch 200B amplifier (Molecular Devices); signals were low-pass filtered at 10 kHz, sampled at 50–100 kHz and acquired with the software Axograph X (Axograph Scientific). For action potential–evoked command waveforms, 100 kHz sampled voltage waveforms were obtained from previous work[13]. Five representative current-clamp recordings from the apical dendrites (170 and 550 µm distance from the soma), the soma, AIS and distal axon were aligned and averaged to generate a single command waveform for each location. The resting potential, action potential amplitude and half-width were as follows: axonal control action potential, −77 mV, 106 mV and 287 µs; 10-s-long subthreshold depolarized axonal action potential, −62 mV, 68 mV and 498 µs; backpropagating action potential at 170 µm, −77 mV, 72 mV and 717 µs; backpropagating action potential at 550 µm, −72 mV, 33 mV and 3.2 ms. The internal four-pole Bessel filter of the amplifier was set to 100 kHz, and current signals obtained through an external eight-pole Bessel low-pass filter set to 20 kHz. The temporal delay caused by the external filter was determined to be ~50 µs and currents were therefore *post hoc* offset to a similar negative delay. Voltage and current signals were sampled at 100 kHz and averaged from 10–50 individual sweeps. An on-line P/N (P/–5) protocol was applied to minimize leak and residual capacitive currents.

Na^+ current was isolated by adding the Ca^{2+}, K^+ and HCN channel blockers Cd^+ (200 µM), 4-aminopyridine (5 mM, Sigma-Aldrich), XE991 (10 µM, Tocris) and ZD-7288 (20 µM, Tocris) to the bath solution, whereas K^+ current was isolated by replacing 4-aminopyridine in this solution with tetrodotoxin (0.5 µM, Alomone Labs). For dendritic recordings, additional K^+ currents were blocked by replacing 20 mM NaCl with equimolar tetraethylammonium chloride (Sigma-Aldrich). For whole-cell axonal K^+ current recordings, about 80–90% series resistance compensation in combination with <10 µs time lag was used. The K^+ reversal potential during all recordings was estimated to be −98.4 ± 4.2 mV ($n = 5$), consistent with predictions based on external and internal K^+ concentrations (3 mM outside, 135 mM inside; −100.3 mV at 33 °C). Steady-state activation and inactivation curves were constructed from peak currents after conversion to conductance by using the experimentally determined K^+ reversal potential of −98 mV, normalized to the maximum conductance, and fitted with a single Boltzmann equation. All data were obtained at 33 ± 2 °C. Membrane potentials have been corrected for a −12-mV liquid junction potential.

The Hodgkin-Huxley models of fast-activating axonal K^+ currents. The K^+ current, I_K, was defined as described previously[18] and extended by adding inactivation mechanisms. Given that the inactivation of axonal K^+ channel currents during long depolarizations to +28 mV for 60 s could be well approximated with two exponential components (data not shown), two populations of K^+ channels with different inactivation kinetics were assumed

$$I_K = \bar{g}_{h1}(V - V_{rev})n^x h_1 + \bar{g}_{h2}(V - V_{rev})n^x h_2$$

$\bar{g}_{h1}$ and $\bar{g}_{h2}$ denote the peak conductance of the slowly and rapidly inactivating current component, respectively, n indicates the activation gate, x denotes the number of activation gates, h_1 and h_2 represent the inactivation gates, V represents the membrane potential, and V_{rev} denotes the reversal potential of −98 mV. The alternative assumption of two inactivation gates in a single K^+ channel, $I_K = \bar{g}(V - V_{rev})n^x h_1 h_2$, which might represent N- and C-type inactivation[36], did not describe the data well (data not shown).

The activation and inactivation gates of the axonal K^+ model followed the differential equation[18]

$$\frac{dn}{dt} = \alpha_n(1-n) - \beta_n n$$
$$\frac{dh_1}{dt} = \alpha_{h1}(1-h_1) - \beta_{h1}h_1$$
$$\frac{dh_2}{dt} = \alpha_{h2}(1-h_2) - \beta_{h2}h_2$$

and the voltage-dependent rates were defined as[18,34]

$$\alpha_n = \frac{-A_{\alpha,n}(V + B_{\alpha,n})}{\exp\left(-\frac{V + B_{\alpha,n}}{C_{\alpha,n}}\right) - 1}$$
$$\beta_n = A_{\beta,n}\exp\left(-\frac{V}{C_{\beta,n}}\right)$$
$$\alpha_{h1} = A_{\alpha,h1}\exp\left(-\frac{V}{C_{\alpha,h1}}\right)$$
$$\beta_{h1} = \frac{A_{\beta,h1}}{\exp\left(-\frac{V + B_{\beta,h1}}{C_{\beta,h1}}\right) + 1}$$

For the rapidly inactivating channels, the rates of inactivation and the recovery from inactivation were multiplied by the same factor (f_{h2})

$$\alpha_{h2} = f_{h2}\alpha_{h1}$$
$$\beta_{h2} = f_{h2}\beta_{h1}$$

The ZHA model of axonal K^+ currents. To test whether a state model could reproduce the currents better, we analyzed the ZHA model[23], which is characterized by 15 closed and one open state. We omitted the closed state (C_{15}) that was introduced to explain the rapid flickering of openings in single-channel recordings. The inactivation was added to this model as described for the Hodgkin-Huxley formalism (that is, n^X is replaced by the open state of the ZHA model in the K^+ current described above). The ZHA state model was defined as previously described[23] (**Supplementary Fig. 2g**), where the rate constants are defined as

$$\alpha = \alpha_0 e^{z\alpha FV/RT}$$
$$\beta = \beta_0 e^{z\beta FV/RT}$$
$$\gamma = \gamma_0 e^{z\gamma FV/RT}$$
$$\delta = \delta_0 e^{z\delta FV/RT}$$

where z is the equivalent charge movement for the transition, F is Faraday's constant, R is the universal gas constant and T is the absolute temperature. Despite the increased complexity of this model, the predictions of the ZHA model were only marginally better than the n^8 Hodgkin-Huxley model (**Supplementary Fig. 2c–e**). In addition, the n^8 Hodgkin-Huxley model reproduced the action potential–evoked currents better than the ZHA model (**Fig. 4b** and **Supplementary Fig. 2f**).

Estimation of the parameters of the K^+ channel models. The Hodgkin-Huxley-model consisted of 13 free parameters. The number of activation gates was set to values between 1 and 128 or was alternatively used as an additional 14th free parameter, yielding 6.53 as the optimal number of activation gates (**Supplementary Fig. 2e**). The ZHA model consisted of 17 free parameters, but the parameters of the inactivation gates were fixed to the values estimated from the Hodgkin-Huxley model with eight activation gates (n^8), resulting in 11 free parameters (**Supplementary Table 1**). For the Hodgkin-Huxley models, the K^+ currents were calculated analytically[18]. For the ZHA model, the currents were calculated by numerical integration as described for vesicle state models previously[47].

For both the Hodgkin-Huxley models and the ZHA model, the steady-state inactivation curve was calculated from the peak current of the second test pulse, identical to the evaluation of the experimental data.

As an unbiased measure of the deviation of the simulated from the recorded currents, the sum of squared differences (χ^2) was calculated as follows: for the activation, deactivation and inactivation (that is, 10-s depolarizing steps as well as the subsequent 0.6-s test step to +58 mV) currents, each current value of each trace was compared with the corresponding simulated current. The resulting three χ^2 values for activation, deactivation and inactivation were weighted by the inverse of the product of a squared representative current value (1 nA throughout), the number of traces and the number of sampled currents in each trace. The second pulse of the inactivation protocol (60 of 1,060 current values) was weighted by a factor of 10 to better capture the kinetics of these mechanistically informative parts of the currents. The three χ^2 values from the steady-state activation and inactivation curve and the recovery from inactivation curve were weighted with the inverse of the number of points in the corresponding curve. This resulted in six χ^2 values that were comparable in size (**Supplementary Fig. 2**). For convenience, the final χ^2 values were multiplied by 100. The optimal free parameters of the models were estimated as described for vesicle state models previously[47]. All simulations to determine the channel parameters were implemented in C++ (Xcode 3.0, Developer Tools; OSX, Apple). To test the ability of the models to reproduce the action potential evoked currents, we implemented the channel models in NEURON simulation environment (v7.2)[48] with NEURON extension NMODL, and calculated the currents in a single compartment that was voltage clamped with the corresponding action potential waveform potential.

Morphology-based model of a L5 pyramidal neuron. Morphology-based cell simulations used Neurolucida (MBF Bioscience) reconstructions of *in vitro* or *in vivo*-labeled L5 pyramidal neurons (**Figs. 4d** and **6a**,**c**) and were imported into the NEURON simulation environment. Spines were incorporated by decreasing the specific R_m (15,000 Ω cm^2) and increasing C_m (1.0 μF cm^{-2}) 1.5-fold in all dendritic compartments. Specific axial resistivity, R_i, was 80.0 Ω cm throughout all compartments. Myelination of internodal sections was represented by increasing R_m threefold and decreasing C_m sixfold, leading to a conduction velocity in the primary axons of 3.53 m s^{-1}, consistent with previous estimates[13,33]. The diameter of all myelinated internodal sections was set to 1.7 μm to match the end of the reconstructed AIS (1.7 μm, at 55 μm from the soma). NoRs were set to be smaller than internodal regions (1.3-μm diameter, 1-μm length) and incorporated every 80 μm. The reversal potential of the leak conductance was set to −90 mV, resulting in a resting membrane potential at the soma of −79 mV. Segment length was adjusted to be below 10% of the alternating current length constant, λ_{AC}, at 1 kHz for each section[48]. Simulations were run with integration time steps (dt) between 5 and 10 μs. For the 10-s lasting simulations with subthreshold depolarization, dt was increased to 10 ms during this period.

Ion channels in the morphology-based model. Na^+ currents were described by two eight-state models developed at the soma and the axon of hippocampal granule cells[24] and reproduced the experimentally recorded action potential evoked Na^+ currents well (**Fig. 4c**). Voltage shifts of Na^+ channel models, accounting for differences in the Donnan and liquid junction potentials and the voltage dependence of inactivation between the whole-cell and isolated-patch configuration, were applied as previously described[24]. That is, for both somatic and axonal Na^+ channel models, the activation was shifted by 10 mV and the inactivation by 22 mV in the depolarized direction. In addition, to match the experimentally observed action potential threshold of −62 mV in the AIS[49] and to reproduce the experimentally observed subthreshold depolarization of ~15 mV without continuous action potential firing, the activation and inactivation of the Na^+ channels at the soma were further depolarized by 2 mV.

K^+ currents were described by three K^+ channel models: a high-voltage delayed type of non-inactivating model with properties similar to K_v2 channels[50], a low voltage–activated non-inactivating K^+ model reflecting K_v7 channels and the newly developed n^8 Hodgkin-Huxley model reflecting axonal K_v1 channels. To reproduce the effect of subthreshold depolarization on action potential-broadening (**Fig. 5**), we right-shifted and left-shifted the activation and inactivation of the newly developed axonal n^8 Hodgkin-Huxley model by 10 mV and 5 mV, respectively. This might reflect uncertainties in the assumed Donnan and liquid junction potentials (12 mV). Alternatively, it could indicate that, during subthreshold depolarizations, additional modification of the membrane conductance occurred as a result of Ca^{2+}-dependent conductances[51,52]. Furthermore, Ca^{2+}-dependent K^+ channels[50], low- and high-voltage Ca^{2+} channels[50], and I_h channels[53] were added to the model. The K^+ and Na^+ equilibrium potentials were set to −98 and +55 mV, respectively.

Channel density in the morphology-based model. To estimate the Na^+ and K^+ channel density in the AIS, we used the axonal action potential recorded at the cut-end AIS of the reconstructed cell (**Fig. 4d**) as a template. Both K^+ and Na^+ current densities, $\bar{g}_K$ and $\bar{g}_{Na}$, respectively, were systematically varied over a large range ($\bar{g}_K$ = 400–10,000 pS μm^{-2}, $\bar{g}_{Na}$ = 2,000–35,000 pS μm^{-2}) and four distinct parameters of the resulting AIS action potentials were analyzed (**Fig. 4e** and **Supplementary Fig. 3**). Mathematica 7.0 (Wolfram Research) was used to automatically executed NEURON simulations with systematically varying parameters and to determine the action potential parameters from the simulated traces. For each of the combinations of the investigated parameters, the injected current amplitude was automatically increased until an action potential was elicited within 5 ms of the onset of the current injection, defined by a rate of rise of the voltage in the AIS and the soma of >50 V s^{-1} (ref. 49). Although the amplitude, voltage threshold and maximum rate of rise (dV/dt) were largely dependent on the density of the axonal Na^+ channels, the action potential half-width was primarily determined by $\bar{g}_K$ (**Supplementary Fig. 3**). Superposition of the experimentally observed target ranges (**Supplementary Fig. 3**) revealed that high channel densities are required to reproduce action potentials in the AIS with realistic properties ($\bar{g}_K$ = 2,000 pS μm^{-2}, $\bar{g}_{Na}$ = 7,000 pS μm^{-2}). On the basis of these results, our standard distribution of axonal $\bar{g}_K$ was a linear increase with distance from the soma until the end of the AIS from 0–2,000 pS μm^{-2}, with a slope of 34.5 pS μm^{-1}, determined by experimentally measured distribution[13]. The high $\bar{g}_{Na}$ of 7,000 pS μm^{-2} was independent of the assumed Na^+ channel kinetics (**Supplementary Fig. 4**) and nearly threefold higher than in previous L5 models[46]. Although this discrepancy may be surprisingly large, we found that it was completely accounted for by an incorrect temperature scaling of the Na^+ conductance implemented in a Hodgkin-Huxley model of Na^+ channels[46,50], leading to an underestimation of Na^+ channel density. In addition to these K^+ and Na^+ models, both NoR and AIS compartments contained low voltage–activated non-inactivating K_v7 channel with a density of 21 pS μm^{-2}. The $\bar{g}_{Na}$ in the reconstructed collaterals of the *in vitro* and *in vivo* L5 thick-tufted pyramidal neurons (ranging between 0.3–0.5 μm in diameter) was uniform set to 500 pS μm^{-2} to obtain a conduction velocity of ~0.42 m s^{-1}, near the experimentally determined conduction velocities for intracollateral axons[54]. Collaterals also contained the axonal n^8 K^+ channel model with $\bar{g}_K$ set to 400 pS μm^{-2}, yielding action potential half-widths of 250 μs.

The channel densities in the soma and the dendrites were based on previously established models of a L5 pyramidal neuron[46,50]. In the soma, the K^+ current was represented by the low voltage–activated non-inactivating model[50] (100 pS μm^{-2}), our axonal n^8 Hodgkin-Huxley model (100 pS μm^{-2}) and a K_v7 channel model (3 pS μm^{-2}). To reproduce the amplitude and rate of rise of the somatic action potential, we set $\bar{g}_{Na}$ to 500 pS μm^{-2}. In the dendrites, the K^+ current was primarily simulated by the K_v2-like high voltage–activated K^+ model[50] (3 pS μm^{-2}), which is the abundant component of the dendritic K^+ current[55]. In addition, a small component of the K_v1-like n^8 model was implemented in the dendrites[56] (0.3 pS μm^{-2}). Both K^+ models decreased in peak conductance density exponentially from the soma to the dendrites (that is, from 100 to 3 and from 100 to 0.3, respectively) with a space constant of 30 μm in both apical and basal dendrites[57]. K_v7 channels were uniform in density (3 pS μm^{-2}). Na^+ channel density in distal dendrites ($\bar{g}_{Na,dend}$) was set to 20 pS μm^{-2} and decreased linearly from the soma to the dendrites (that is, 500 to 20 pS μm^{-2}) over the first 300 μm for the apical and 60 μm for basal dendrites, respectively[57]. These K^+ and Na^+ distributions could account for both the recorded Na^+ and K^+ current amplitudes (**Figs. 1** and **6**) and for realistic distance-dependent attenuation of the backpropagating action potential (**Supplementary Fig. 5e**,**f**).

Energy consumption in the morphology-based model. To estimate the subcellular distribution of the ATP consumption, we used the NEURON extension NMODL to integrate the Na^+ influx per membrane area for each segment of the NEURON models and assumed that three Na^+ ions were extruded per

doi:10.1038/nn.3132

ATP molecule[1] (**Fig. 6**). The total ATP consumption in the gray matter for the soma, dendrites, AIS and myelinated primary axon was directly determined from the simulations in the NEURON model by summating of the Na^+ charge in all the segments of the corresponding compartments of the reconstructed cell. In addition, NMODL extensions were developed to calculate for each segment the charge separation ratio and the excess Na^+ entry ratio. The resulting values were analyzed and plotted as NEURON range variables (**Fig. 6a** and **Supplementary Fig. 5c**,**d**). For the energy calculations, the myelinated axon length was extrapolated to 4.5 mm; 1.5 mm accounts for the distance to the corpus callosum and another 3 mm was based on the average white-matter axon length in rodents[58].

The ATP consumption of thick- and slender-tufted L5 neurons (**Fig. 6e**) was estimated by scaling the ATP consumption in the axons and dendrites of the thick-tufted L5 neuron (**Fig. 6c**,**d**) with the corresponding length distribution of the axonal and dendritic arborization determined in thick- and slender-tufted L5 neurons ($n = 3$ each)[27]. To estimate the other costs related to action potential propagation (**Fig. 6g**), we estimated the number of presynaptic boutons as 7,776, based on an interbouton distance of 2.9 μm[27] and an axonal length of 2.26 cm of our *in vivo*–reconstructed thick-tufted L5 neuron. Assuming a release probability of 0.25 (ref. 59), 1,944 vesicles are therefore released per action potential. Taking presynaptic Ca^{2+} influx, glutamate recycling and postsynaptic glutamate currents into account, 16,400 ATP molecules have been associated with the release of one vesicle in the cortex[1], resulting in 319×10^6 ATP molecules per action potential for synaptic transmission. Next, the costs for action potential propagation and synaptic transmission were scaled with the average *in vivo* action potential frequency of 3.77 Hz[28] for thick-tufted neurons. Housekeeping costs were assumed to be one-fourth of the total energy use in the gray matter of the cerebral cortex[1]. The cost for resting membrane potential was determined directly from the models.

Statistics. Statistical significance between groups was tested using GraphPad Prism (v.4.0) by applying one-way ANOVA followed by Tukey multiple comparison *post hoc* tests. Differences between two groups were tested using paired or unpaired two-tailed Student's *t* tests. The cut-off significance level (P) was 0.05.

46. Kole, M.H.P. *et al.* Action potential generation requires a high sodium channel density in the axon initial segment. *Nat. Neurosci.* **11**, 178–186 (2008).
47. Hallermann, S. *et al.* Bassoon speeds vesicle reloading at a central excitatory synapse. *Neuron* **68**, 710–723 (2010).
48. Carnevale, N.T. & Hines, M.L. *The NEURON book* (Cambridge University Press, Cambridge, 2005).
49. Kole, M.H.P. & Stuart, G.J. Is action potential threshold lowest in the axon? *Nat. Neurosci.* **11**, 1253–1255 (2008).
50. Mainen, Z.F. & Sejnowski, T.J. Influence of dendritic structure on firing pattern in model neocortical neurons. *Nature* **382**, 363–366 (1996).
51. Awatramani, G.B., Price, G.D. & Trussell, L.O. Modulation of transmitter release by presynaptic resting potential and background calcium levels. *Neuron* **48**, 109–121 (2005).
52. Christie, J.M., Chiu, D.N. & Jahr, C.E. Ca^{2+}-dependent enhancement of release by subthreshold somatic depolarization. *Nat. Neurosci.* **14**, 62–68 (2011).
53. Kole, M.H.P., Hallermann, S. & Stuart, G.J. Single Ih channels in pyramidal neuron dendrites: properties, distribution, and impact on action potential output. *J. Neurosci.* **26**, 1677–1687 (2006).
54. Lohmann, H. & Rörig, B. Long-range horizontal connections between supragranular pyramidal cells in the extrastriate visual cortex of the rat. *J. Comp. Neurol.* **344**, 543–558 (1994).
55. Guan, D., Tkatch, T., Surmeier, D.J., Armstrong, W.E. & Foehring, R.C. K_V2 subunits underlie slowly inactivating potassium current in rat neocortical pyramidal neurons. *J. Physiol. (Lond.)* **581**, 941–960 (2007).
56. Bekkers, J.M. & Delaney, A.J. Modulation of excitability by α-dendrotoxin–sensitive potassium channels in neocortical pyramidal neurons. *J. Neurosci.* **21**, 6553–6560 (2001).
57. Keren, N., Bar-Yehuda, D. & Korngreen, A. Experimentally guided modeling of dendritic excitability in rat neocortical pyramidal neurones. *J. Physiol. (Lond.)* **587**, 1413–1437 (2009).
58. Braitenberg, V. & Schüz, A. *Cortex: Statistics and Geometry of Neuronal Connectivity* (Springer, London, 1998).
59. Markram, H., Lübke, J., Frotscher, M., Roth, A. & Sakmann, B. Physiology and anatomy of synaptic connections between thick tufted pyramidal neurones in the developing rat neocortex. *J. Physiol. (Lond.)* **500**, 409–440 (1997).